RSC Applied Interfaces

ROYAL SOCIETY OF CHEMISTRY

PAPER

View Article Online
View Journal | View Issue

Cite this: *RSC Appl. Interfaces*, 2024, **1**, 573

SARS-CoV-2 inactivation: assessing the efficacy of GO-anchored filters *versus* various commercial masks†

Md. Saidul Islam, ‡[ab] Nurun Nahar Rabin,‡[ab] Mst Monira Begum,[c] Nonoka Goto,[a] Ryuta Tagawa,[a] Mami Nagashima,[d] Kenji Sadamasu,[d] Kazuhisa Yoshimura,[d] Junko Matsuda,[e] Yoshihiro Sekine, [af] Terumasa Ikeda*[c] and Shinya Hayami *[abg]

The outbreak of the coronavirus disease 2019, caused by the severe acute respiratory syndrome coronavirus 2 (SARS-CoV-2), posed a significant global health threat. As a result, face masks became widely adopted as a preventive measure to mitigate the spread of the virus. However, the effectiveness of different mask materials in filtering and inactivating SARS-CoV-2 varies. In this study, we investigated the efficacy of graphene oxide (GO)-anchored filters in inactivating SARS-CoV-2 and compared their performance to various commercially available masks under controlled laboratory conditions. Our findings demonstrated that GO-anchored filters exhibited superior SARS-CoV-2 inactivation efficiency compared to all tested commercial masks. The enhanced efficacy of GO-anchored filters is attributed to the unique physicochemical properties of graphene oxide, which enable the physical capture of viral particles and virucidal activity through mechanisms such as oxidative stress and membrane disruption. These results highlight the potential of GO-anchored filters as a promising material for developing high-performance face masks with superior viral filtration and inactivation capabilities. This knowledge is valuable for informing public health measures and guiding the development of effective personal protective equipment (PPE) to combat current and future pandemics.

Received 15th December 2023,
Accepted 26th February 2024

DOI: 10.1039/d3lf00250k

rsc.li/RSCApplInter

Introduction

The coronavirus disease 2019 (COVID-19), stemming from the severe acute respiratory syndrome coronavirus 2 (SARS-CoV-2), swiftly disseminated across the globe following its inception in late 2019. Its impact has been profound, wreaking havoc on global health, economies, and societies.[1,2] SARS-CoV-2 transmission mechanisms and dynamics have been well studied in past years.[3–5] It has been recognized that the virus primarily spreads through respiratory droplets and various modes of human contact. When an infected individual talks, coughs, or sneezes, respiratory droplets containing the virus are released into the air. These droplets can be inhaled by people in proximity, leading to infection. Additionally, the virus can remain in the air in smaller aerosolized particles, making poorly ventilated or enclosed spaces potential areas for transmission through inhalation.[5] Another standard transmission route is contact with contaminated surfaces, where the virus can survive for hours to days.[6] People can contract the virus by touching these contaminated surfaces and subsequently touching their face, allowing the virus to enter through the eyes, nose, or mouth. Asymptomatic or pre-symptomatic carriers can unknowingly transmit the virus, emphasizing the need for preventive measures to curb the spread of the disease. Masks have played a crucial role in mitigating the virus spread; they primarily function as a barrier that helps prevent respiratory droplets containing the virus from being released into the air when an infected person talks, coughs, sneezes or even breathes. This is particularly important because many individuals infected with SARS-CoV-2 may not show

[a] *Department of Chemistry, Faculty of Advanced Science and Technology, Kumamoto University, 2-39-1 Kurokami, Kumamoto 860-8555, Japan. E-mail: hayami@kumamoto-ua.c.jp*
[b] *Institute of Industrial Nanomaterials, Kumamoto University, 2-39-1 Kurokami, Chuo-ku, Kumamoto 860-8555, Japan*
[c] *Division of Molecular Virology and Genetics, Joint Research Center for Human Retrovirus Infection, Kumamoto University, Kumamoto 860-0811, Japan. E-mail: ikedat@kumamoto-u.ac.jp*
[d] *Tokyo Metropolitan Institute of Public Health, Tokyo 169-0073, Japan*
[e] *International Research Center for Hydrogen Energy, Kyushu University, 744 Motooka, Fukuoka, Fukuoka, 819-0395, Japan*
[f] *Priority Organization for Innovation and Excellence, Kumamoto University, 2-39-1 Kurokami, Chuo-ku, Kumamoto 860-8555, Japan*
[g] *International Research Center for Agricultural and Environmental Biology (IRCAEB), 2-39-1 Kurokami, Chuo-ku, Kumamoto 860-8555, Japan*
† Electronic supplementary information (ESI) available. See DOI: https://doi.org/10.1039/d3lf00250k
‡ Equal contribution.

symptoms but can still spread the virus.[7] Therefore, when a significant proportion of the population wears masks consistently and correctly, it can reduce the overall spread of the virus within the community. As a result, by wearing masks and following other preventive measures, communities can help prevent rapid infection spikes that might necessitate strict lockdowns (Scheme 1).

It is worth noting that commercial face masks have played a vital role in the past few years in preventing the spreading of SARS-CoV-2. Nevertheless, a considerable virus spread has been observed, even after wearing the mask, forcing them to impose strict lockdowns and substantial economic losses. In particular, the commercially available face mask is manufactured to protect individuals from dust, pollen, or bacteria attacks. Notably, the pore size of the mask materials is suitable to avoid dust or pollen with large particle sizes. In addition, some active materials used in specific masks allow for inhabiting bacterial infections. In sharp contrast, the properties of the virus, including SARS -CoV-2 are distinct from those of dust, pollen, or bacteria. The virus particle size is small enough to pass through the pores of mask materials.[8,9] Nevertheless, the commercial mask can help prevent the virus from spreading through absorption of the virus particle on the mask surface and block the airborne droplets, with a possible spreading risk. Therefore, developing suitable mask materials is important to protect against future virus-driven pandemics. Utilizing anti-virus ingredients as additives in the mask might be a viable solution for improving the mask's performance for spreading the virus infection.

Previously, we demonstrated the potential of GO in effectively inactivating SARS-CoV-2 through a multifaceted mechanism.[10] In particular, the mechanism involves the adsorption of SARS-CoV-2 onto the surface of GO nanosheets, followed by the inactivation of the virus through the decomposition of its spike (S) protein. This process effectively neutralizes the virus and prevents its ability to infect host cells. The surface of GO carries a negative charge, which interacts electrostatically with the positively charged surface of SARS-CoV-2, facilitating the adsorption of the virus onto GO nanosheets. This interaction disrupts the structural integrity of the viral particles, as observed through *in situ* transmission electron microscopy (TEM), inhibiting their function and preventing infection. Additionally, enzyme-linked immunosorbent assay (ELISA) observations reveal that GO can directly interact with viral proteins, particularly the S glycoprotein critical for viral entry into host cells, leading to the destruction of key protein structures.[10] The high surface area and unique physicochemical properties of GO facilitate efficient binding and subsequent inactivation of SARS-CoV-2, offering a potential strategy for developing effective antiviral materials and coatings.[10] Moreover, the increment in the hydroxyl functional groups at a higher pH of GO has more anti-SARS-CoV-2 activity than that of acidic or neutral conditions.[11] Some other recent works also provide the theoretical and practical possibility of GO-based materials as a platform to combat current and future pandemics.[12–14] In the present work, we demonstrate the SARS-CoV-2 inactivation of GO-anchored filters and compare the inactivation efficiency with the commercially available face mask.

Scheme 1 The role of mask to mitigate the virus spreading.

Experimental

The isolation and titration of the BA.5 variant (strain TKYS14631; GISAID ID: EPI_ISL_12812500) has been described previously.[15,16] This variant was used to investigate the antiviral activity of different commercial masks and GO samples against SARS-CoV-2. Eight different commercial face masks include hydro silver titanium mask (Hyd [$AgTiO_2$]), copper oxide mask, silver ion ceramic mask, special dolomite "CDM (BR-p3, contain Ca and Mg) mask, pioneer mask, CLEANXIA mask, sharp mask and surgical mask (using Viablock non-woven fabric) were purchased from the local market. GO was purchased commercially (from Nippon Shokubai Co. Ltd.) with an oxidation degree of 33% and used without further purification. A commercial polytetrafluoroethylene (PTFE) filter (pore size: 0.22 μm) was utilized to prepare the GO-anchored filters with varying concentrations. GO-modified filter was prepared by passing GO with two different concentrations (i) 0.5 mg mL^{-1}, 1 mL named as GO filter (low conc.), and ii) 1 mg mL^{-1}, 1 mL named as GO filter (high conc.) through the filter under reduced pressure, followed by drying in air. To measure the anti-SARS-CoV-2 performance of the PTFE filter, a commercial PTFE syringe filter (PTFE filter, pore size: 0.22 μm) was utilized to filter the cell culture supernatant containing the SARS-CoV-2 virus. The supernatant was initially drawn into a syringe and passed through the PTFE filter. After the filtration, the cell culture supernatant was used to perform the plaque assay. The anti-SARS-CoV-2 performance of the mask components or GO-anchored filters was measured by replacing the PTFE filter with the corresponding mask or GO filter. However, we did not see a big volume loss after the filtration. Plaque assays were conducted to measure the antiviral efficiency of the GO-anchored mask against the BA.5 variant, as reported previously.[10,11,15–19] The details about the experimental procedure are shown in the ESI.†

Results and discussion

The surface morphology and chemical properties of the commercial masks used in the current work are shown in

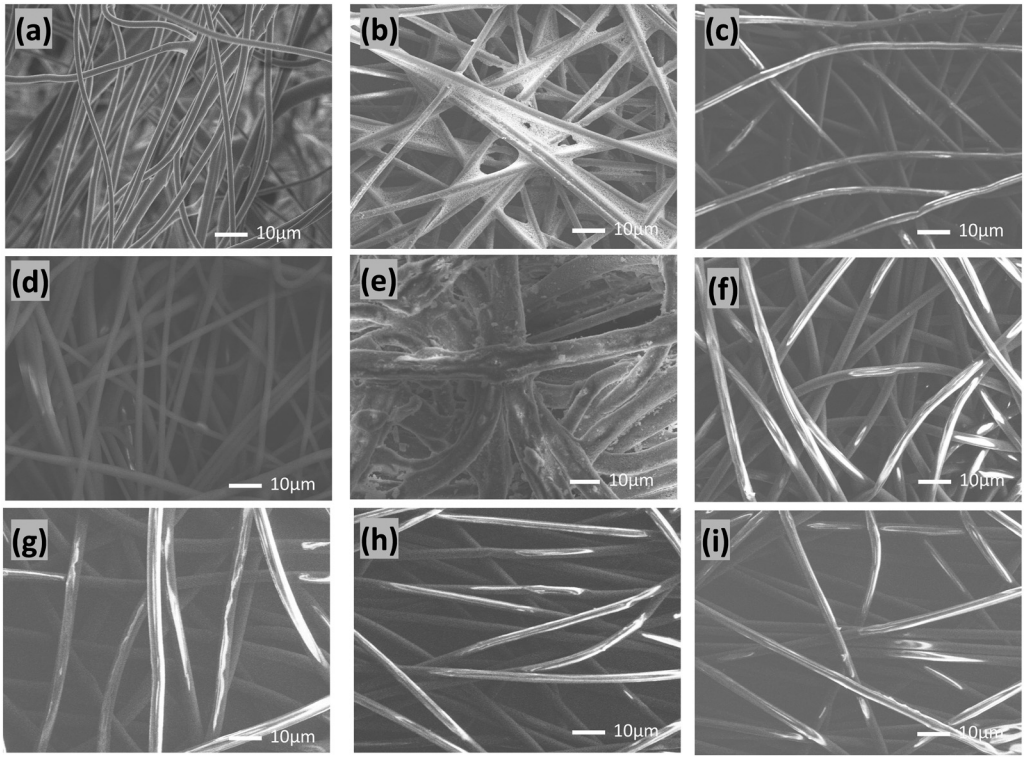

Fig. 1 Surface morphology of commercially available mask utilized in the current work. SEM images of a) commercial PTFE filter, b) hydro silver titanium mask, c) copper oxide mask, d) silver ion ceramic mask, e) special dolomite "CDM mask", f) Pioneer mask, g) CLEANXIA mask, h) sharp mask, and i) surgical mask.

Fig. 1 and S1.† Fig. 1(a–i) shows the scanning electron microscope (SEM) images of the commercial PTFE syringe filter, hydro silver titanium mask, copper oxide mask, silver ion ceramic mask, special dolomite CDM mask, pioneer mask, CLEANXIA mask, SHARP mask, and surgical mask (using Viablock non-woven fabric), respectively. The SEM images reveal the typical surface characteristics of each mask, providing insights into their structural morphology. Additionally, the presence of active materials attached to the masks is clearly observed in the images, signifying potential functionalities beyond the structural aspect. To further understand the chemical composition of these masks, corresponding energy dispersive X-ray (EDX) spectra were obtained (Fig. S1†). The EDX spectra confirm the presence of specific elements associated with the active materials incorporated into the masks. For instance, in the Hydro silver titanium mask (Fig. S1a†), silver (Ag) and titanium (Ti) are observed at 7.55 and 0.11 atomic percent (At%), respectively. Simultaneously, peaks corresponding to carbon (C), oxygen (O), aluminium (Al), phosphorus (P), and calcium (Ca) are detected, indicating the complex composition of the mask. These results emphasize the diversity in the elemental composition of the masks, underscoring the incorporation of various active materials and supporting the need for a comprehensive understanding of surface morphology and chemical composition in evaluating the effectiveness and potential applications of these commercial masks. Detecting foreign elements further implies the intentional addition of specific functionalities to enhance the performance of these protective masks.

GO was characterized using atomic force microscopy (AFM), Raman spectroscopy, and powder X-ray diffraction (PXRD) techniques.[20–24] AFM analysis (Fig. S2a†) revealed the nanosheet structure of GO, while the corresponding height profile (Fig. S2b†) demonstrated a thickness of approximately 1 nm, consistent with a monolayer configuration. This thinness suggests effective exfoliation of the GO sheets, facilitating their high dispersion in aqueous solutions. Raman spectroscopy (Fig. S2c†) further elucidated the structural features of GO. Two prominent peaks were observed: the "D band" and the "G band." The D band, located around 1350 cm^{-1}, corresponds to the breathing mode (a_{1g}) of sp^3 carbon atoms and indicates the presence of structural defects or disorder in the graphene lattice. The G band, positioned at approximately 1580 cm^{-1}, is associated with the in-plane bond stretching motion (e_{2g}) of pairs of sp^2 carbon atoms and signifies the graphitic nature of GO. The presence of both bands confirms the successful formation of GO. Moreover, PXRD analysis revealed characteristic peaks at 10.2, consistent with the typical diffraction pattern of graphene oxide. These diffraction peaks further support the presence of GO and validate its structural integrity. However, the interaction and attachment of GO with the PTFE filter were comprehensively characterized using advanced microscopy techniques, including Scanning Transmission Electron Microscopy-High Angle Annular Dark Field (STEM-

HAADF), Scanning Transmission Electron Microscopy-Bright Field (STEM-BF), and Transmission Electron Microscopy (TEM). Cross-section analyses of the pristine PTFE filter and the GO-anchored commercial PTFE filter were conducted, and the results are presented in Fig. 2 and S3.† Fig. 2a and b depict STEM-HAADF and STEM-BF images, respectively, of the cross-section of the pristine PTFE filter. The filter's non-woven fiber (NW fiber) structure is clearly visible, providing a baseline for comparison. Fig. 2c–e illustrate the GO-anchored commercial PTFE filter cross-section's corresponding STEM-HAADF, STEM-BF, and TEM images. These images reveal the attachment of the PTFE filter's particles with GO. Notably, the thickness of the attached GO layer is calculated as 1 nm, as shown in Fig. 2e. The attachment of GO to the PTFE filter particles was further substantiated through selected area electron diffraction (SAED) analysis, as depicted in Fig. S3.† Specifically, three distinct areas, labelled as a, b, and c, were selected for SAED pattern examination. The SAED pattern obtained from area b exhibited a characteristic pattern indicative of GO, thereby confirming the presence of attached GO sheets with the nonwoven fiber of the filter. Conversely, areas a and c did not display such characteristic patterns.

This discrepancy underscores the specificity of GO attachment to certain regions of the PTFE filter particles, as evidenced by the absence of GO-related diffraction patterns in areas lacking GO anchoring. The SAED analysis conclusively establishes that the attached sheet within the PTFE filter particles corresponds to GO, affirming a robust anchoring of GO onto the filter materials. This finding underscores the efficacy and reliability of the GO-modified filter in potential applications requiring enhanced filtration efficiency, particularly in the context of viral containment such as SARS-CoV-2.

To assess the anti-SARS-CoV-2 efficacy of various commercial masks and GO-anchored PTFE filters, the BA.5 variant was employed and is shown in Fig. 3 and 4, respectively. Plaque assays were conducted before and after filtering the virus solution, as outlined in the experimental section while maintaining consistent conditions across all other parameters. Fig. 3 shows that typical cytopathic effects were observed without a mask or filter.[10,19] The filtration process using commercial masks PTFE filters reduced the plaque-forming units (PFUs) compared to that without mask or filter and shows the efficiency increasing order of No filter < CLEANXIA mask < surgical mask < hydro silver titanium mask < silver ion ceramic mask < pioneer mask < PTFE filter < copper oxide mask < special dolomite CDM mask < sharp mask (Fig. 3). On the other hand, a superior anti-SARS-CoV-2 performance exhibited by the GO-anchored PTFE filter compared to the PTFE is particularly noteworthy (Fig. 4). The enhanced antiviral performance of the GO-anchored PTFE filters is likely due to GO's superior antiviral properties, complemented by the absorption of virus particles on the mask surface.[10] Moreover, the increased concentration of GO proved to be more effective than the lower concentration in enhancing the anti-SARS-CoV-2 performance. The only difference between the pristine PTFE filter and the GO-anchored PTFE filter is the introduction of GO. Therefore, the enhanced performance can be attributed to the introduction of GO in the PTFE filter.

The current findings suggest that all mask samples exhibit superior antiviral performance compared to those without masks or filters. However, variations in anti-viral efficiency among different masks may be attributed to differences in the antiviral capabilities of the active materials integrated into the mask samples. The enhanced effectiveness of different masks in combating COVID-19 can be attributed to the phenomenon of virus adsorption onto the mask surface. Even though the average pore size of commercial masks is typically larger than that of the virus particle, studies have

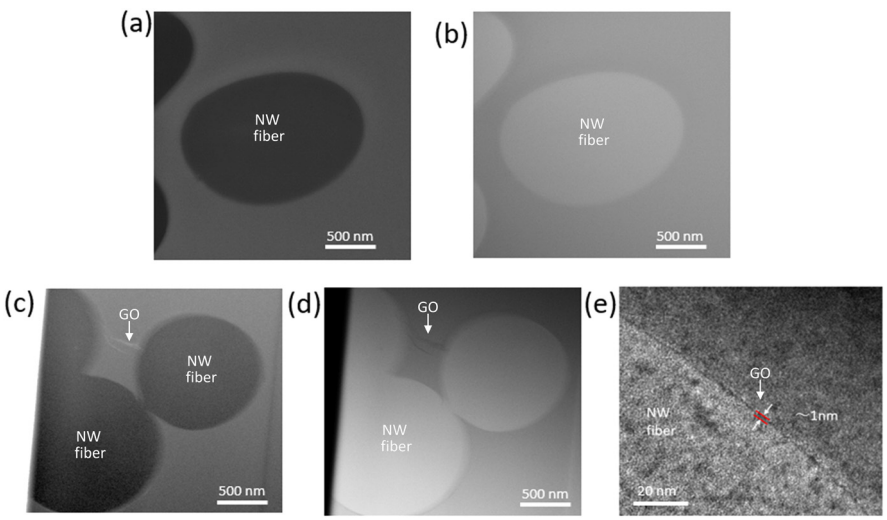

Fig. 2 Characterization GO anchored commercial PTFE filter. a) STEM-SAADF image of pristine PTFE filter, b) STEM-BF image of pristine PTFE filter, c) STEM-SAADF image of GO anchored PTFE filter, d) STEM-BF image of GO anchored PTFE filter, and e) TEM image of GO anchored PTFE filter.

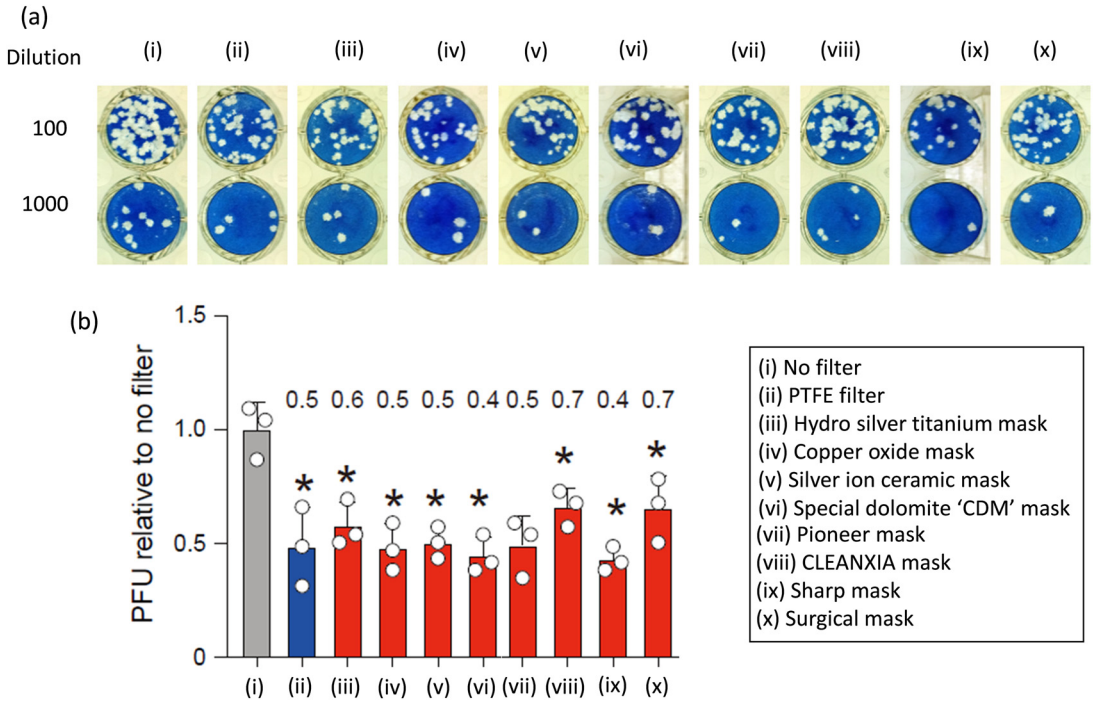

Fig. 3 Antiviral effects of PTFE filter and different commercial masks on the BA.5 variant. Panel (a) shows representative pictures of plaque assay. Panel (b) is representative plaque assay data of three independent experiments with average ± standard deviation of plaque-forming unit (PFU) relative to no filter (n = 3). Statistical significance was assessed using a one-way ANOVA and Dunnett's test. The asterisks (*) indicate $p < 0.05$ compared with the H_2O (no filter). Fold change compared with no filter was mentioned above each bar.

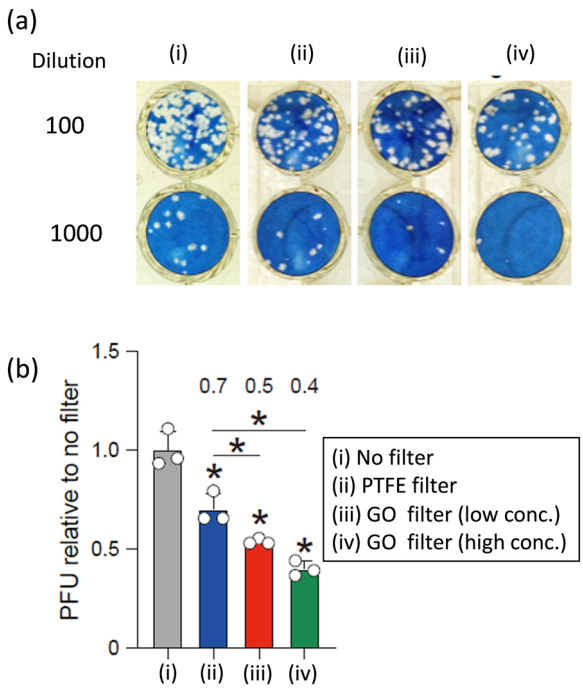

Fig. 4 Antiviral effects of pristine PTFE filter and GO-anchored PTFE filters on the BA.5 variant. Panel (a) shows representative pictures of plaque assay. Panel (b) is representative plaque assay data of three independent experiments with average ± standard deviation of plaque-forming unit (PFU) relative to no filter (n = 3). Statistical significance was assessed using a one-way ANOVA and Dunnett's test. The asterisks (*) indicate $p < 0.05$ compared with the H_2O (no filter) or PTF filter. Fold change compared with no filter was mentioned above each bar.

consistently demonstrated significant virus deactivation when using these masks. This observation suggests that while the pores may not physically block all virus particles, the mask material still effectively captures and deactivates the virus. We hypothesize that this effectiveness is due to the adsorption of virus particles onto the surface of the mask. As infected individuals exhale or cough, respiratory droplets containing virus particles contact the mask surface. The mask's material then absorbs these virus particles, preventing their further transmission. Furthermore, commercial masks are designed to effectively block airborne droplets, reducing the risk of virus spread.

We appreciate that the phrase "99.9% effective" on the commercial mask typically refers to the mask's ability to filter out a certain percentage of airborne particles, including dust, allergens, bacteria, and other potentially harmful substances. However, it is essential to differentiate between filtering out general airborne particles and filtering out virus particles, especially in the context of respiratory viruses like the ones that cause COVID-19. Airborne particles such as dust, pollen, and bacteria vary in size, and here are their typical particle size ranges. The coarse dust particles are greater than 10 μm while fine dust particles are between 2.5 to 10 μm, pollen particles lie between 10 to 100 μm, and most bacteria particles are within the range of 0.5 to 5 μm. Virus particles, including those responsible for respiratory illnesses, are significantly smaller than typical airborne particles. SARS-CoV-2 particles are tiny, typically ranging from 0.06 to 0.14 μm, and easily pass through the pore size of the filter

materials of the mask. Therefore, achieving a high filtration efficiency for particles of this size is technically challenging. Herein, we succeeded in enhancing the antiviral performance of the PTFE filter through GO as additives.

Designing a face mask with optimum anti-virus ability and suitable for spreading the virus during a pandemic has received considerable attention and research focus. Understanding the efficacy of various commercial masks in inactivating SARS-CoV-2 is paramount for public health. With the virus continuing to circulate and new variants emerging, it is crucial to identify masks that offer the highest level of protection to individuals and communities. Such information can help guide public health policies and recommendations on mask-wearing protocols, especially in high-risk environments and during disease outbreaks. It is worth noting that understanding the cytotoxic effects of materials used in face masks is crucial for ensuring safety. Despite reports indicating that GO exhibits insignificant cytotoxicity below a certain concentration, there is ongoing debate regarding its *in vivo* toxicity.[25,26] Nevertheless, we believe collaborative efforts between material scientists and health experts are vital for advancing our understanding of GO's safety profile and refining methods to reduce cytotoxicity. These strategies include surface modification with biocompatible molecules or polymers to reduce its interaction with cells, size control to produce smaller and less toxic GO sheets, functionalization with specific chemical groups to alter its biological interactions, combination with other materials to create hybrid composites with reduced cytotoxicity, dose optimization, and thorough *in vitro* and *in vivo* studies to assess its biocompatibility. By employing these approaches, scientists aim to harness the unique properties of GO while ensuring its safety for biomedical and technological applications.

Conclusions

In summary, developing suitable respiratory masks with sufficient antiviral ability is crucial in preventing future pandemics. Through the advancements in material with optimal antiviral protections, masks could significantly reduce the transmission of respiratory viruses, such as SARS-CoV-2 and influenza virus. Compared to the commercial masks, the GO-anchored PTFE filter shows enhanced anti-SARS-CoV-2 properties. The current findings can be attributed to the anti-SARS-CoV-2 ability of the GO and imply the potential of GO in the field of virus inactivation and personal protective equipment, including face masks. This study provides valuable insights into the effectiveness of commercial masks and antiviral materials as additives to inhibit SARS-CoV-2 particles. Incorporating GO into filters results in substrate-enhanced antiviral properties surpassing commercial masks, presenting a potent strategy to mitigate the transmission of SARS-CoV-2 and other viruses. Moreover, the current research outputs suggest that incorporating materials with antivirus capabilities as mask additives signifies a promising avenue for utilizing diverse antivirus materials in crafting effective masks for future pandemics.

Author contributions

S. H., T. I., and Y. S. designed the study and main conceptual ideas. M. S. I., N. N. R., N. G., and R. T. prepared and characterized the various Mask and graphene oxide anchored mask samples. M. N., K. S., and K. Y. provided the resources and collected the data. M. M. B. did the plaque assay Experiment. J. M. did the STEM-SAADF, STEM-BF, and TEM analysis. M. S. I. and N. N. R. interpreting the results and preparing the original draft manuscript. S. H., Y. S., and T. I. revised the manuscript critically for important intellectual content. All authors discussed the results and commented on the manuscript.

Conflicts of interest

"There are no conflicts to declare".

Acknowledgements

This project was funded by the Institute of Industrial Nanomaterials (IINa) fusion project fund, Kumamoto University, Japan (to M. S. I.), a KAKENHI Grant-in-Aid for Scientific Research (Grant No. JP17H01200) from the Ministry of Education, Culture, Sports, Science, and Technology, Japan (to S. H.), JST A-STEP (JPMJTM20SL, to T. I.), a JSPS KAKENHI Grant-in-Aid for Scientific Research C (22 K07103, to T. I.), JSPS Leading Initiative for Excellent Young Researchers (LEADER) (to T. I.), Mochida Memorial Foundation for Medical and Pharmaceutical Research (to T. I.), The Naito Foundation (to T. I.), Takeda Science Foundation (to T. I.), Shin-Nihon Foundation of Advanced Medical Research (to T. I.), Waksman Foundation of Japan (to T. I.), and an intramural grant from Kumamoto University COVID-19 Research Projects (AMABIE) (to T. I.).

Notes and references

1 P. Zhou, X.-L. Yang, X.-G. Wang, B. Hu, L. Zhang, W. Zhang, H.-R. Si, Y. Zhu, B. Li, C.-L. Huang, H.-D. Chen, J. Chen, Y. Luo, H. Guo, R.-D. Jiang, M.-Q. Liu, Y. Chen, X.-R. Shen, X. Wang, X.-S. Zheng, K. Zhao, Q.-J. Chen, F. Deng, L.-L. Liu, B. Yan, F.-X. Zhan, Y.-Y. Wang, G.-F. Xiao and Z.-L. Shi, *Nature*, 2020, **579**, 270–273.

2 Y.-C. Wu, C.-S. Chen and Y.-J. Chan, *J. Chin. Med. Assoc.*, 2020, **83**, 217–220.

3 E. C. Lee, N. I. Wada, M. K. Grabowski, E. S. Gurley and J. Lessler, *Science*, 2020, **370**, 406–407.

4 V. Stadnytskyi, C. E. Bax, A. Bax and P. Anfinrud, *Proc. Natl. Acad. Sci. U. S. A.*, 2020, **117**, 11875–11877; L. Morawska and J. Cao, *Environ. Int.*, 2020, **139**, 105730.

5 R. Zhang, Y. Li, A. L. Zhang, Y. Wang and M. J. Molina, *Proc. Natl. Acad. Sci. U. S. A.*, 2020, **117**, 14857–14863; Martin Z.

Bazant and J. W. M. Bush, *Proc. Natl. Acad. Sci. U. S. A.*, 2021, **118**, e2018995118.
6 N. van Doremalen, T. Bushmaker, D. H. Morris, M. G. Holbrook, A. Gamble, B. N. Williamson, A. Tamin, J. L. Harcourt, N. J. Thornburg, S. I. Gerber, J. O. Lloyd-Smith, E. de Wit and V. J. Munster, *N. Engl. J. Med.*, 2020, **382**, 1564–1567.
7 M. A. Johansson, T. M. Quandelacy, S. Kada, P. V. Prasad, M. Steele, J. T. Brooks, R. B. Slayton, M. Biggerstaff and J. C. Butler, *JAMA Netw. Open*, 2021, **4**, e2035057.
8 K. Violaki, A. Nenes, M. Tsagkaraki, M. Paglione, S. Jacquet, R. Sempéré and C. Panagiotopoulos, *npj Clim. Atmos. Sci.*, 2021, **4**, 63.
9 V. R. Després, J. A. Huffman, S. M. Burrows, C. Hoose, A. S. Safatov, G. Buryak, J. F. Nowoisky, W. Elbert, M. O. Andreae, U. Pöschl and R. Jaenicke, *Tellus B*, 2012, **64**, 015598.
10 M. Fukuda, M. S. Islam, R. Shimizu, H. Nasser, N. N. Rabin, Y. Takahashi, Y. Sekine, L. F. Lindoy, T. Fukuda, T. Ikeda and S. Hayami, *ACS Appl. Nano Mater.*, 2021, **4**, 11881–11887.
11 M. S. Islam, M. Fukuda, M. J. Hossain, N. N. Rabin, R. Tagawa, M. Nagashima, K. Sadamasu, K. Yoshimura, Y. Sekine, T. Ikeda and S. Hayami, *Nanoscale Adv.*, 2023, **5**, 2413–2417.
12 V. Palmieri and M. Papi, *Nano Today*, 2020, **33**, 100883.
13 G. B. Ramaiah, A. Tegegne and B. Melese, *Mater. Today: Proc.*, 2021, **47**, 4357–4363.
14 M. A. Unal, F. Bayrakdar, H. Nazir, O. Besbinar, C. Gurcan, N. Lozano, L. M. Arellano, S. Yalcin, O. Panatli, D. Celik, D. Alkaya, A. Agan, L. Fusco, S. Suzuk Yildiz, L. G. Delogu, K. C. Akcali, K. Kostarelos and A. Yilmazer, *Small*, 2021, **17**, 2101483.
15 I. Kimura, D. Yamasoba, T. Tamura, N. Nao and T. Suzuki, *et al.*, *Cell*, 2022, **185**, 3992–4007.e3916.
16 MST M. Begum, K. Ichihara, O. Takahashi, H. Nasser, M. Jonathan, K. Tokunaga, I. Yoshida, M. Nagashima, K. Sadamasu, K. Yoshimura, K. Sato and T. Ikeda, *bioRxiv*, 2023, preprint, DOI: **10.1101/2023.10.03.560628**.
17 A. Saito, T. Irie, R. Suzuki, T. Maemura, H. Nasser, K. Uriu and Y. Kosugi, *et al.*, *Nature*, 2022, **602**, 300–306.
18 R. Suzuki, D. Yamasoba, I. Kimura, L. Wang, M. Kishimoto, J. Ito and Y. Morioka, *et al.*, *Nature*, 2022, **603**, 700–705.
19 D. Yamasoba, I. Kimura, H. Nasser, Y. Morioka, N. Nao, J. Ito, K. Uriu, M. Tsuda, J. Zahradnik and K. Shirakawa, *et al.*, *Cell*, 2022, **185**, 2103–2115.e2119.
20 M. S. Islam, J. Yagyu, Y. Sekine, S. Sawa and S. Hayami, *Mater. Adv.*, 2022, **3**, 3418–3422.
21 M. Fukuda, M. S. Islam, Y. Shudo, J. Yagyu, L. F. Lindoy and S. Hayami, *Chem. Commun.*, 2020, **56**, 4364–4367.
22 M. R. Karim, M. S. Islam, K. Hatakeyama, M. Nakamura, R. Ohtani, M. Koinuma and S. Hayami, *J. Phys. Chem. C*, 2016, **120**, 21976–21982.
23 J. Yagyu, M. S. Islam, Y. Shudo, M. Fukuda, H. Ushijima, J. Ohyama, S. Ida, L. F. Lindoy and S. Hayami, *ACS Appl. Energy Mater.*, 2021, **4**, 6296–6301.
24 K. Wakata, M. S. Islam, M. R. Karim, K. Hatakeyama, N. N. Rabin, R. Ohtani, M. Nakamura, M. Koinuma and S. Hayami, *RSC Adv.*, 2017, **7**, 21901–21905.
25 M. Kucki, P. Rupper, C. Sarrieu, M. Melucci, E. Treossi, A. Schwarz, V. León, A. Kraegeloh, E. Flahaut, E. Vázquez, V. Palermod and P. Wick, *Nanoscale*, 2016, **8**, 8749.
26 Y. Li, H. Yuan, A. V. D. Bussche, M. Creighton, R. H. Hurt, A. B. Kane and H. Gao, *Proc. Natl. Acad. Sci. U. S. A.*, 2013, **110**, 12295.